Sphingomyelin is critical in organizing phosphoinositide dynamics during phagocytic uptake of *Mycobacterium tuberculosis*

Patrick Niekamp[*1,2], Gaelen Guzman[*1], Hans Leier[1], Ali Rashidfarrokhi[3], Veronica Richina[4], Joost CM Holthuis[2], Fikadu G. Tafesse[1#]

[*]These authors contributed equally.

[1]Department of Molecular Microbiology and Immunology, Oregon Health & Science University, 3181 SW Sam Jackson Park Road, Portland, OR 97239.

[2]Biology & Chemistry Department, University of Osnabrück, Fachbereich Biologie/Chemie, Barbarastrasse 13, 49076 Osnabrück, GERMANY.

[3]Department of Pathology and Department of Medicine, New York University Langone, 550 First Avenue, MSB 594, New York, NY 10016.

[4]Department of Biomedicine University Hospital Basel Hebelstrasse 20 4031 Basel Switzerland.

[#]Correspondence: tafesse@ohsu.edu

Abstract

Infection by Mycobacterium tuberculosis (Mtb) represents a significant global health burden. Mtb invades alveolar macrophages through phagocytosis, and cholesterol has been shown as essential for this invasion, but the roles played by other host lipids remained poorly understood. As such, this study investigated the role of sphingolipids in the early stages of Mtb infection. To this end, we use chemical and genetic perturbations of the sphingolipid biosynthetic pathway to show that sphingolipids are required for efficient phagocytosis of Mtb. We define this dependency to the presence of cellular sphingomyelin and show that sphingolipid depletion does not affect other forms of endocytosis. We furthermore show that the turnover dynamics of phosphoinositides and recruitment of small GTPases to the phagosomal synapse are perturbed upon blockade of sphingolipid synthesis. Finally, we show that the clustering of innate immune receptors such as Dectin-1 and the concurrent exclusion of the regulatory phosphatase CD45 at the phagocytic synapse is defective in sphingolipid-deficient cells. This work represents an essential step in understanding the coalescence of host-pathogen interactions that give rise to Mtb as a global pathogen.

32

33 **Introduction**

34 The etiologic agent behind an estimated 10 million new cases of tuberculosis and 1.6 mil-
35 lion deaths in 2017 alone, *Mycobacterium tuberculosis* (Mtb) has established itself as a highly
36 effective and insidious pathogen[1,2]. Mtb invades alveolar immune cells through phagocytosis, and
37 wields an extensive repertoire of effector molecules that operate to dampen the immune response,
38 reprogram the host lipidome, and promote long-term intracellular survival[3,4]. As an intracellular
39 pathogen, Mtb necessarily interacts with its host along numerous lipid interfaces throughout its
40 infectious lifecycle. Understanding the biological roles of host lipids during infection may illumi-
41 nate novel routes of therapeutic strategies to prevent the onset and spread of tuberculosis[5].

42 In most contexts, phagocytosis is critical for clearing dead and effete cells, and serves
43 as a first line of defense against microbial pathogens. This process culminates in the engulf-
44 ment and internalization of target particles, which are subsequently degraded following conver-
45 gence of the phagosome with the lysosome[6]. In the context of pathogen clearance, uptake by pro-
46 fessional phagocytes (primarily monocytes, macrophages, and dendritic cells) results in a robust
47 inflammatory response and antigen presentation that may contribute to an adaptive immune re-
48 sponse[7]. For example, our previous work shows that phagocytic uptake of *Candida albicans* is
49 essential for the clearance of infection *in vivo*[8]. In contrast, Mtb is highly adept at subverting its
50 own degradation to survive within phagosome-derived compartments through an array of mecha-
51 nisms. As one example, this pathogen inhibits the Ca^{2+}-dependent fusion of the phagosome to the
52 lysosome by disrupting the activity of sphingosine kinase[6,9]. Despite extensive literature on the
53 host-pathogen interactions of Mtb, the specific functional roles played by host lipid species at the

54 site of initial phagocytic uptake of Mtb have remained relatively unstudied. In particular, struc-
55 tural and signaling functions played by sphingolipids at the cell membrane and within the phago-
56 some during Mtb infection are unknown.

57 Sphingolipids are a complex family of membrane lipids that contain a sphin-
58 goid base. Sphingomyelin constitutes a significant fraction of the total lipid composition of the
59 exoplasmic leaflet of the plasma membrane and plays critical roles in the organization of lipid
60 rafts[10,11]. A growing body of literature shows that sphingolipids mediate functions beyond existing
61 as membrane barrier components: members of this family accumulate in lipid rafts and act as sec-
62 ondary messengers within the cell[12–14]. These signaling functions are relevant to many biological
63 processes that span from apoptosis and autophagy to stress response and inflammation in many (if
64 not all) mammalian cell types[15–17]. In one example, the cellular proportions of ceramide and
65 spingosine-1-phosphate have been shown to act as a rheostat that determines cell survival under
66 stress. Notably, it has been shown that the biosynthetic flow of sphingolipids through the Golgi
67 creates a regulatory feedback loop that controls the levels of phosphatidylinositol-4-phosphate,
68 though interactions outside of the *trans*-Golgi network are unknown[18].

69 Prior work has investigated the roles played by sphingolipids during the phagocytosis of
70 other particles – contradictory reports describe the effect of sphingolipid depletion during phago-
71 cytosis. In one example, we have previously reported that cellular sphingolipids are critical for the
72 *in vivo* clearance of *Candida albicans* infection through phagocytosis by macrophages[8]. In con-
73 trast, depletion of cellular sphingolipids enhances phagocytic uptake of opsonized particles[19]. To-
74 gether, these differing results suggest that the roles played by sphingolipids during phagocytosis
75 may be pathogen or particle specific, based on the specific ligands decorating a particle[20]. It has

76 been shown previously that phagocytosis of Mtb is cholesterol-dependent[21]. However, the role of
77 sphingolipids during uptake of Mtb is unknown.

78 Here, we employed chemical and genetic tools to manipulate levels of sphingolipids in
79 mammalian phagocytes, and infected them using an mCherry-expressing reporter strain of H37Rv
80 Mtb. We first show that host sphingolipid depletion reduces the capacity of Mtb to invade host
81 cells through phagocytosis – but that other mechanisms of cellular uptake are unaffected. We show
82 that sphingolipid-depleted cells display defects in phagocytic signaling including a defect in the
83 activation and recruitment of the small GTPases Rac1 and CD42 to the phagocytic cup. We further
84 show that the turnover of phosphoinositidyl-4,5-*bis*phosphate is impaired during phagocytosis in
85 sphingolipid depleted cells. Finally, we show that sphingolipid depletion results in defective ag-
86 gregation of phagocytic receptors at the site of particle engagement. Together, these data demon-
87 strate the need for intact host sphingolipid biosynthesis during the initial stages of Mtb infection.
88 These data also suggest a novel mechanism through which sphingolipids coordinate phosphoinosi-
89 tide-mediated signaling during phagocytosis of Mtb.
90

91 **Results**

92

93 **Manipulating sphingolipid biosynthesis in mammalian phagocytes using genetic and chemi-**
94 **cal tools**

95 To answer our central question – "Are sphingolipids required for the phagocytic uptake of
96 Mtb?" – we sought to inhibit sphingolipid biosynthesis in established phagocytic models. We first
97 used a chemical approach to inhibition using the compounds myriocin and fumonisin B1. As de-
98 picted in Figure 1A, the initial and rate limiting step of sphingolipid synthesis is the production of
99 the sphingoid base through the condensation of serine and palmitoyl-CoA, and is performed by
100 the enzymatic complex serine palmitoyltransferase (SPT)[22]. The atypical amino acid myriocin
101 (Myr) specifically blocks the activity of SPT, and thereby blocks total *de novo* synthesis of sphin-
102 golipids[8]. The fungal toxin fumonisin B1 (FB1) acts several steps downstream in the sphingolipid
103 biosynthetic pathway by blocking the activity of ceramide synthase[8]. As the central nexus of sphin-
104 golipid synthesis, ceramide is converted into many classes of higher sphingolipids - including
105 sphingomyelin, glycosphingolipids, and galactosylceramides[23,24].

106 To verify the reported effects of myriocin and fumonisin B1, we used thin layer chroma-
107 tography to visualize the incorporation of 3-L-[^{14}C]-serine into sphingolipid species in RAW
108 246.7, THP-1, DC 2.4, and U937 cells following 3-day treatment with 15 μM Myr and 5μM FB1
109 (Figure 1D and Supplementary Figure 1). Across all cell lines, treatment with these compounds
110 resulted in significant reduction of sphingolipid content, without disrupting phosphatidylserine
111 content – demonstrating the specificity and potency of these compounds (Figure 1E and F).

112 As an orthogonal method to the above chemical inhibitors, we used CRISPR/Cas-9 editing
113 to generate Sptlc2 knockouts in both RAW 264.7 and DC 2.4 cells. Sptlc2 is one of the members

114 of the SPT complex, and we previously reported that this knockout phenocopies myriocin treat-
115 ment[8]. We validated loss of protein expression by Western blotting (Figure 1C). We used thin
116 layer chromatography to visualize the incorporation of 3-L-[^{14}C]-serine into lipid species in both
117 wildtype and Sptlc2$^{-/-}$ RAW 246.7 and DC2.4 cells. In both cases, Sptlc2 deletion significantly
118 reduced sphingolipid content without altering phosphatidylserine levels (Figure 1E and F and Sup-
119 plemental Figure 1).

120 To further examine the lipid composition of sphingolipid deficient cells, we performed
121 mass spectroscopy-based lipidomic analysis of RAW 264.7 macrophages following treatment with
122 chemical inhibitors and Sptlc2 knockout. We examined cellular levels of sphingosine, ceramide,
123 sphingomyelin, glucosylceramide. As expected, both myriocin and Sptlc2 knockout result in sig-
124 nificant reduction of all sphingolipid species (Figure 1 G-J). In fumonisin B1 treated cells, we
125 observe reduction of all sphingolipid species downstream of ceramide synthesis (the point of inhi-
126 bition along the biosynthetic pathway), but we observe a concordant increase in sphingosine (syn-
127 thesized upstream of ceramide), as reported previously (Figure 1G-J)[25].

128 Notably, we observe that myriocin and fumonisin B1 treatment, as well as Sptlc2 knockout,
129 do not result in the total ablation of cellular sphingolipid content. This is at least partially attribut-
130 able to the activity of the sphingolipid salvage pathways, through which cells may acquire sphin-
131 golipids from additives in media – primarily serum. As we describe below, cells grown in the
132 absence of serum additive quickly die when sphingolipid biosynthesis is inhibited.

133

134

135

136

137 **Sphingolipid depletion has no significant effect on cell morphology or cell division.**

138 What effect does the inhibition of sphingolipid synthesis have on basal cellular functions?
139 We hoped to characterize the changes to morphology and cell growth resulting from myriocin and
140 fumonisin B1 treatments, and Sptlc2 knockout.

141 We show that in RAW 264.7, DC 2.4, THP-1, and U937 cells, there are minimal decreases
142 in replication rates following three-day treatments with 5μM myriocin and 15μM fumonisin B1,
143 and following Sptlc2 knockout (Supplementary Figure 2B and C and data not shown). Similarly,
144 we use brightfield microscopy to show that there are no obvious defects of cellular morphology
145 over the course of inhibitor treatments, or following Sptlc2 knockout (Supplementary Figure 2A
146 and data not shown). As noted above, serum is an essential additive when culturing sphingolipid-
147 deficient cells. We observe that RAW 264.7 Sptlc2 knockout cells rapidly die in the absence of
148 serum, whereas wildtype cells remain relatively healthy after three days without serum (data not
149 shown). We believe that cells deficient in sphingolipid biosynthesis acquire sphingolipids from
150 media at only the minimal level to allow cell growth, as their overall sphingolipid content is sig-
151 nificantly lower than in wildtype cells (Figure 1D-J).

152 Notably, when grown in the presence of serum, the major phenotype observed in these cells
153 over the course of this study is in the rate of phagocytic uptake of certain particles, as we have
154 reported previously for DC 2.4 knockout cells[8]. We observe that Sptlc2$^{-/-}$ RAW 264.7 cells display
155 a significant reduction in the capacity to phagocytose Zymosan A particles (data not shown).

156 Having thus characterized the effects inhibition of sphingolipid biosynthesis, we hoped to
157 use these inhibitory mechanisms (myriocin, fumonisin B1, and Sptcl2 knockout) to address the
158 question: "Are sphingolipids an essential host factor in the phagocytic uptake of Mtb?"

159

160 **Cells deficient in sphingolipid biosynthesis display reduced capacity to phagocytose Mtb.**

161 To investigate the role of sphingolipids during phagocytic uptake of Mtb, we used Myr and
162 FB1 to block sphingolipid synthesis in RAW 264.7, THP-1, DC 2.4, and U937 cells. We then
163 infected cells with an mCherry-expressing strain of Mtb to quantify rates of phagocytosis. Figure
164 2A depicts the experimental and analysis workflow. Briefly, cells were infected at a multiplicity
165 of infection (MOI) of 10 for two hours, after which cells were fixed and stained with Alexa Fluor
166 488-conjugated phalloidin and with DAPI (to visualize F-actin at cell boundary and nuclei, respec-
167 tively). Fluorescence microscopy was used to quantify uptake efficiency through automated count-
168 ing of cell number (by nuclei) and internalized bacteria (red fluorescent particles within green cell
169 boundary). We report uptake efficiency as the ratio of the total number of internalized Mtb parti-
170 cles against the number of identified nuclei, and normalized the uptake rate of treated cells to that
171 of untreated cells to address variability between biological replicates. In all cell models analyzed,
172 we observed a statistically significant reduction in Mtb uptake of approximately 50% following
173 treatment with myriocin, and approximately 40% for fumonisin B1 (Figure 2B-I). Similarly, the
174 knockout of Sptlc2 resulted in approximately 50% of wildtype uptake in both RAW 264.7 and DC
175 2.4 cells (Figure 2B-I). These results suggest that the maintenance of total cellular sphingolipid
176 levels through active sphingolipid biosynthesis is required for efficient phagocytic uptake of Mtb
177 across four model cell lines and irrespective of the mechanism of inhibition. We next sought to
178 identify the exact species required for efficient Mtb uptake.

179 **Sphingolipid-depleted cells are permissive to virus that utilizes phagocytosis-like processes**

180 Are the effects of sphingolipid depletion restricted to phagocytic uptake? To answer this
181 question, we performed parallel infections of RAW264.7 wildtype and Sptlc2 knockout cells using
182 a fluorescent reporter strain of Herpes Simplex Virus-1 (HSV) encoding a fusion of viral protein

183 VP26 and mCherry[26]. HSV is an enveloped virus that gains entry to host cells through the phago-
184 cytosis-like process of macropinocytosis, and the viral receptors have been shown to be nectin-1
185 (also known as herpesviruses entry mediator)[27,28]. It has been shown that HSV entry is dependent
186 on cholesterol-rich lipid rafts and dynamin2[29]. At 12-hours post-infection, we visualized and quan-
187 tified rates of infection using fluorescence microscopy as described above. Because the VP26-
188 mCherry reporter construct localizes to the nucleus, we did not stain cells using phalloidin and
189 instead used the colocalization of DAPI with mCherry as a measure of infection. We observe that
190 there is no significant difference in the infection rates of wildtype and Sptlc2-/- cells, suggesting
191 that sphingolipids play no significant role in the entry of HSV-1 (Figure 2J and K). These data
192 demonstrate that endocytic pathways are functional in sphingolipid-deficient cells, suggesting a
193 specific role for sphingolipids in phagocytosis of bacterial pathogens such as Mtb by immune
194 cells.

195 **Cells deficient in sphingomyelin biosynthesis display reduced Mtb infection**

196 Which sphingolipid confers this phenotype? Because sphingomyelin is highly enriched to
197 the exoplasmic leaflet of the plasma membranes, we hypothesized that this lipid species is respon-
198 sible for reduced Mtb uptake in cells depleted of total sphingolipids[10,23,38]. Because sphingomyelin
199 is a terminal branch of the sphingolipid biosynthetic pathway, and its synthesis mainly mediated
200 by the enzyme sphingomyelin synthase 1 (SGMS1), cells may be depleted of this specific lipid
201 species through CRISPR/Cas9-mediated knockout of this gene. Two SGMS1 CRISPR knockout
202 clones of U937 cells were kindly provided to us by the lab of Dr. Sebastian Virriera Winter, iso-
203 lated as previously described[39]. Using these SGMS1 knockouts, we performed Mtb uptake assays
204 as described above. We found that, despite minor clonal differences, these cells are significantly

205 reduced in their capacity to uptake Mtb to a similar degree as to that of cells deficient in the bio-
206 synthesis of all sphingolipids (Figure 3A and B). Together with the above results, these data sug-
207 gest that sphingomyelin is particularly crucial for the phagocytic uptake of particles such as Mtb.
208

209 **Sphingolipid depleted cells are defective in activation of small GTPases Cdc42/Rac1.**

210 What is the mechanism through which sphingolipids enable phagocytic uptake of Mtb?
211 Phagocytosis is strictly regulated through a signaling network that involves the dynamic activation
212 and recruitment of both enzymes (such as GTPases, kinases, and phosphatases) and lipids – par-
213 ticularly several phosphatidylinositol species. As depicted in Figure 4A, the GTPases Cdc42 and
214 Rac1 are activated via phosphorylation following engagement of phagocytic receptors to patho-
215 genic particles such as Mtb[30]. The activation of these GTPases builds as a particle is fully engaged
216 by a phagocytic receptor; once a particle is engulfed, Cdc42 and Rac1 are deactivated via
217 dephosphorylation as the phagocytic signaling cascade is terminated[30]. We hypothesized that in-
218 hibiting sphingolipid biosynthesis would prohibit the activation of Cdc42 and Rac1 during phag-
219 ocytosis.

220 To address this hypothesis, we transfected wildtype and Sptlc2$^{-/-}$ RAW 264.7 macrophages
221 with a fluorescent biosensor consisting of the fusion of YFP to the p21-binding domain of the p21-
222 activated kinase (PBD(PAK)-YFP)[31,32]. Endogenous PAK is recruited from the cytosol to specif-
223 ically bind to phosphorylated Cdc42 and Rac1 at the site of phagosome formation, and diffuses
224 back to the cytosol upon the dephosphorylation of these GTPases –this biosensor enables the vis-
225 ualization of spatiotemporal GTPase activation[31,32]. Following transfection, we infected cells using
226 the phagocytic model particle Zymosan A at an MOI of 10 and performed live imaging to visualize
227 the localized activation of these GTPases.

228 *Due to the BSL3 requirements of Mtb, we used the model phagocytic particle Zymosan A*
229 *in these live imaging experiments. Zymosan A particles are composed of chains of fungus-derived*
230 *β-glucan – which engages the mannose-binding receptor Dectin-1, expressed on professional*
231 *phagocytes*[33]*. We have observed that sphingolipid depletion reduces uptake of Zymosan A to a*
232 *similar degree as to Mtb (ref, data not shown).*

233 We first demonstrate in wildtype RAW 264.7 cells that phosphorylation of Cdc42/Rac1
234 increases upon particle recognition and peaks as a particle is engulfed (Figure 4B and Supplemen-
235 tary Movie 1). Quantifying the enrichment of reporter signal at the site of particle contact versus
236 cytosol signal across at least four cells shows a sharp peak of biosensor recruitment as a particle is
237 engulfed (Figure 4C). In contrast, this activation initially builds in Sptlc2-/- cells at a rate indistin-
238 guishable from wildtype, but we observe poor activation of Cdc42/Rac1 at later timepoints in
239 comparison to wildtype cells (Figure 4B and C and Supplementary Movie 2).

240 From these results, we conclude that in sphingolipid-deficient cells, the initial activation of
241 Cdc42/Rac1 are unaffected – but that this activation fails to peak at high enough levels to fully
242 engulf pathogen-particles. The initial stages of phagocytosis briefly act in a positive feedback loop,
243 in which the engagement of receptor initiates signaling that results in the additional aggregation of
244 receptor and thus further enhances signal. Because the initial stages of phagocytosis are unaffected
245 by deficient biosynthesis of sphingolipids, we hypothesized that an intermediate signaling step is
246 dependent on sphingolipid levels at the cell membrane. We next characterized the activity of down-
247 stream phosphoinositide signaling to explain this observation.

248

249 **Sphingolipid depleted cells are defective in phosphatidylinositol3,4,5-trisphosphate synthe-**
250 **sis.**

251 Do sphingolipids mediate phosphoinositide signaling during phagocytosis? As depicted in
252 Figure 5A, Rho GTPase activation initiates the conversion of phosphatidylinositol-4-phosphate
253 ($PI_{(4)}P$) to phosphatidylinositol-4,5-*bis*phosphate ($PI_{(4,5)}P_2$) at the base of the phagocytic synapse.
254 The accumulation of $PI_{(4,5)}P_2$ is essential to initiate the polymerization of actin filaments that drive
255 the leading edges of the growing phagosome around the particle[31]. Following the leading edge of
256 $PI_{(4,5)}P_2$ production, the enzyme phosphatidylinositol 3-kinase (PI_3K) converts $PI_{(4,5)}P_2$ into phos-
257 phatidylinositol-3,4,5-*tris*phosphate ($PI_{(3,4,5)}P_3$), which initiates a trailing edge of actin disassem-
258 bly at the base of the phagosomal cup. This degradation of $PI_{(4,5)}P_2$ is critical for the full engulfment
259 of the engaged particle, as it drives the pseudopodia around the particle and enables the invagina-
260 tion of the phagosomal cup[7]. To date, there have been no reports tying phosphoinositide signaling
261 to cellular sphingolipid content during phagocytosis. However, sphingolipid and phosphoinositide
262 levels within the Golgi regulate each other in a homeostatic feedback circuit: buildup of sphingo-
263 myelin in the Golgi initiates dephosphorylation of $PI_{(4)}P$, which subsequently reduces the import
264 of cholesterol sphingolipid into the Golgi[18,36]. As such, we hypothesized that sphingolipids play a
265 similar role in phosphoinositide turnover during phagocytosis of Mtb-like particles.
266 To address this hypothesis, we transfected RAW 264.7 wildtype and Sptlc2 knockout cells
267 with biosensors that specifically bind two phosphoinositide species and used live imaging to assess
268 the uptake of Zymosan A particles. The first such biosensor we used consisted of the fusion of
269 GFP to the plekstrin homology (PH) domain of phospholipase C-delta (PLCδ), which selectively
270 binds to $PI_{(4,5)}P_2$ (PH(PLCδ)-GFP)[7]. We show an enrichment of GFP signal to the site of particle
271 engagement as wildtype cells synthesize $PI_{(4,5)}P_2$ following particle recognition, and that this syn-
272 thesis peaks with the engulfment of the particle (Figure 5B and C and Supplemental Movie 3). In
273 Sptlc2 knockout cells, $PI_{(4,5)}P_2$ production is initially the same as in wildtype cells, but fails to

274 build to the same levels as the cells fail to uptake particles (Figure 5B and C and Supplementary
275 Movie 4).

276 Next, we transfected RAW 264.7 cells with a $PI_{(3,4,5)}P_3$ biosensor consisting of the PH do-
277 main of Akt fused to GFP (PH(AKT)-GFP)[37]. We visualize the localization of biosensor signal to
278 show that wildtype cells begin synthesizing $PI_{(3,4,5)}P_3$ early in phagocytosis, and that this synthesis
279 strongly peaks as a particle is fully engulfed (Figure 5D and E and Supplementary Movie 5). How-
280 ever, Sptlc2 knockout cells fail to produce a trailing wave of $PI_{(3,4,5)}P_3$, and thus never reach the
281 levels of synthesis observed in wildtype cells (Figure 5D and E and Supplementary Movie 6).

282 Together, these findings suggest that the inefficiency of Mtb uptake in sphingolipid-defi-
283 cient cells is due to defects in phagocytic signaling resulting from defective phosphoinositide turn-
284 over. At early stages of phagocytosis, there are minimal differences between wildtype and Sptlc2-
285 /- cells – but the knockout cells fail to reach critical thresholds of phosphoinositide signal mole-
286 cules (particularly $PI_{(3,4,5)}P_3$) to drive the full propagation of phagocytosis and thereby fail to up-
287 take particles.

288

289 **The phagocytic receptor Dectin-1 fails to aggregate at the site of particle engagement in**
290 **sphingolipid-deficient cells**

291 As described by Goodridge et al. in 2011, the engagement of phagocytic receptor to ligand
292 initiates the accumulation of receptor to the phagocytic synapse, which results in the physical ex-
293 pulsion of inhibitory phosphatases such as CD45 from the phagocytic synapse and the formation
294 of a lipid raft-like domain[40]. Prior work has shown that the several intracellular pathogens, includ-
295 ing Mtb, induce their uptake in a cholesterol-dependent manner[5,41]. As such, we hypothesized that

296 cellular sphingolipid content is required for the aggregation of the phagocytic receptor Dectin-1 to
297 the site of particle engagement, and the concomitant exclusion of CD45 from the contact site.

298 To address this hypothesis, we transiently transfected wildtype and Sptlc2$^{-/-}$ RAW 264.7
299 macrophages with a GFP-conjugated Dectin-1 construct, and assessed the co-localization of this
300 fluorescent protein with the inhibitory phosphatase CD45 upon treatment with non-fluorescent
301 Zymosan A particles 2 min post incubation. In both wildtype and Sptlc2 knockouts, we find that
302 Dectin-1 in wildtype cells aggregates at the site of contact with Zymosan A, and that the co-local-
303 ization of CD45 with Dectin-1 is significantly reduced in these sites of particle contact (Figure 6A
304 and B). In contrast, the colocalization of Dectin-1-GFP and CD45 in Sptlc2 knockout cells is only
305 minimally reduced (Figure 6A and B). These data suggest that that sphingolipids are required to
306 mediate the dramatic changes in membrane fluidity required for proper phagosomal cup formation
307 and transduction of pro-phagocytic signals (such as phosphatidylinositol turnover).

308 To control against the possibility that deficient sphingolipid biosynthesis results in altered
309 surface expression of CD45 and Dectin-1, we used flow cytometry to compare wildtype and
310 Sptlc2$^{-/-}$ RAW 264.7 cells. We probed cells for endogenous surface protein using APC-conjugated
311 anti-CD45 antibody and FITC-conjugated anti-Dectin-1 antibody. We found agreement in overall
312 fluorescent signal for both wildtype and Sptlc2 knockout cells for both surface markers (Figure
313 6C-F). These results suggest that the overall levels of both CD45 and Dectin-1at the cell surface
314 are unaffected by depletion of sphingolipids.

315

316 **Discussion**

317 In this study, we report that the capacity of Mtb to invade host cells by engagement of
318 phagocytic receptors is significantly dependent on active sphingolipid biosynthesis and the pres-
319 ence of host sphingolipids at the cell membrane. Our central findings are thus: First, the blockade
320 of total sphingolipid synthesis reduces Mtb uptake by approximately 50% – and the specific block-
321 ade of sphingomyelin synthesis produces a phenocopy of this observation. Critically, we show that
322 sphingolipid depletion has no effect on the macropinocytosis of Herpes Simplex Virus – suggest-
323 ing that these cells remain otherwise susceptible to infection via other routes of cellular uptake.
324 Next, we show that several critical stages of phagocytic signaling involving phosphoinositide turn-
325 over are perturbed upon depletion of sphingolipid synthesis, resulting in defective phagosome for-
326 mation. And finally, we show that the clusterring of innate immune receptors such as Dectin-1 and
327 the simultaneous exclusion of regulatory phosphatases CD45 at the phagocytic synapse is defec-
328 tive in sphingolipid-deficient cells.

329 In addition to the initial observations of defective internalization of Mtb by sphingolipid-
330 deficient hosts, we present a possible mechanism through which sphingolipids enable the propa-
331 gation of phagocytic signaling by coordinating phosphoinositide turnover. Upon engagement of
332 phagocytic receptor to cognate ligand, Rho GTPases Rac1 and Cdc42 are activated and initiate the
333 localized production of $PI_{(4,5)}P_2$. This local increase in the concentration of $PI_{(4,5)}P_2$ initiates F-
334 actin polymerization at the base of the forming phagocytic cup, which drives pseudopodia around
335 the particle. Concomitantly, the progression of the pseudopod requires cyclic F-actin disassembly
336 and assembly. This recycling process is driven by a trailing edge of $PI_{(4,5)}P_2$ phosphorylation to
337 $PI_{(3,4,5)}P_3$ via PI3K starting at the base of the phagosomal cup[31]. Because we observe defects in the
338 propagation of this signaling pathway beginning with the production of $PI_{(3,4,5)}P_3$, we argue that

339 sphingolipids, and sphingomyelin in particular, are responsible for coordinating the necessary in-
340 teractions between kinases and their phosphoinositide substrates. One candidate of particular in-
341 terest for further investigation is PI3K, which may require interaction with or membrane tethering
342 by sphingolipids at the site of phagocytic receptor engagement.

343 This study represents, to our knowledge, the first evidence for sphingolipids as regulators
344 of phosphoinositide turnover during phagocytosis. This agrees with prior reports that sphingolipids
345 play roles in phosphoinositide signaling in other contexts. For example, phosphatidylinositol 4-
346 phosphate (PI_4P) has been implicated in the transfer of ceramides from the ER to the Golgi by
347 interacting with the ceramide transfer protein CERT[36]. Additionally, Capasso and colleagues
348 showed that sphingomyelin production triggers dephosphorylation of PI_4P at the trans-Golgi as a
349 negative feedback mechanism, suggesting regulatory interplay that maintains cellular levels of
350 sphingomyelin[18].

351 As a whole, this study demonstrates that sphingolipids are key host factors in infection by
352 Mtb. Phagocytosis in this context represents a double-edged sword: while this immune process is
353 critical for the clearance of many pathogenic particles, Mtb harnesses phagocytosis to gain entry
354 to host cells and establish long-term survival. It may be possible to target a therapeutic to specifi-
355 cally block the interaction between Mtb and host lipids, but this will require more comprehensive
356 understanding of how this lipid class enables Mtb pathogenicity. This study represents an im-
357 portant step in developing our knowledge of the underlying mechanisms of pathogenesis in Mtb
358 infection and contributes to the development of new strategies to fight this ancient pathogen.

359

360

361 **Materials and Methods**

362 **Reagents.**

363 Myriocin and fumonisin B1 were purchased from Cayman Chemical Company. 3-L-
364 [^{14}C]serine was purchased from American Radioactivity. Phorbol 12-myristate 13-acetate (PMA)
365 was purchased from BioLegend. 4% Paraformaldehyde was from Fisher Scientific. Alexa Fluor®
366 488 Phalloidin and Zymosan A (*S. cerevisiae*) BioParticles Alexa Fluor 594 conjugate were pur-
367 chased from Thermo Fisher. Rabbit polyclonal antibody against phospho-PI3 Kinase p85
368 (Tyr458)/p55 (Tyr199) (p-PI3K) (#4228) was purchased from Cell Signaling Technology. Mouse
369 Monoclonal antibody against GAPDH (ab8245) was purchased from Abcam. Anti-rabbit IgG
370 HRP-linked antibody and anti-mouse IgG HRP-linked antibody were purchased from Cell Signal-
371 ing. APC-conjugated, rat monoclonal antibody against CD45 antibody (Clone 30-F11) was pur-
372 chased from Biolegend. FITC-conjugated, rat monoclonal antibody against Dectin-1 (Clone 2A11)
373 was purchased from AbD Serotec. Zombie Aqua™ Fixable Viability Kit (part #77143) was pur-
374 chased from BioLegend and kindly provided by the lab of Dr. Tim Nice. Rat monoclonal blocking
375 antibody against CD16/32 (Clone 93) was purchased from Biolegend and kindly provided by the
376 lab of Dr. Tim Nice.

377 **Plasmids**

378 Active (GTP-bound) Rac1/Cdc42 was detected with PAK(PBD)-YFP, a plasmid encoding
379 the PBD of PAK fused to YFP[32]. $PI(_{4,5})P_2$ was detected with PH(PLCδ)-GFP, a plasmid encoding
380 the PH domain of PLCδ fused to GFP (kindly provided by Grinstein). $PI(_{3,4,5})P_3$ levels were mon-
381 itored by PH(AKT)-GFP, a plasmid encoding the PH domain of AKT fused to GFP[43].

382 The plasmids used for generation of lentivirus consists of the pCDH-CMV(-)-sgRNA plas-
383 mid, the psPAX2 plasmid (packaging) and pMD2.G plasmid (envelope). pCW-Cas9 lentivirus was
384 purchased from Addgene.

385 **Cell culture and drug treatment**

386 THP-1, U937, Raw 264.7 and DC 2.4 cells were routinely cultured in RPMI medium sup-
387 plemented with 10% FBS (Seradigm) and 1% Pen Strep (Gibco). HeLa cells were cultured in
388 DMEM supplemented with 10% FBS and 1% Pen Strep. All cell lines were cultured at 37 °C and
389 5% CO_2. In plating adherent cells (RAW 264.7 and DC 2.4), cells were lifted using 1x 0.25%
390 Trypsin solution (Gibco) and counted using hemocytometer, with Trypan Blue solution (Gibco)
391 for counterstain.

392 THP-1 and U937 cells were differentiated to macrophages by 50ng/ml PMA for 1 day in
393 RPMI medium supplemented with 10% FBS, after which the cells were treated with 5μM myriocin
394 or fumonisin B1 for 3 days in RPMI supplemented with 10% FBS and 1%Pen Strep. RAW 264.7
395 and DC 2.4 cells were treated identically with myriocin and fumonisin B1.

396 **Radio-active labeling and TLC**

397 5.0×10^5 THP-1, U937, RAW 264.7, and DC 2.4 (both wildtype and Sptlc2-/-) cells were
398 seeded into a well of a 6-well plate, differentiated and treated as described above (Cell culture and
399 drug treatment). After 3 days of drug treatment the cells were labeled with 1μCi/ml of 3-L-[^{14}C]-
400 serine for 4 hours in Opti-MEM supplemented with the appropriate drug concentration of myriocin
401 and FB1 and incubated at 37°C. Cells were washed two times with PBS and lipid extraction was
402 done following the Bligh and Dyer method[44]. The methanol/chloroform-lipid extracts were dried
403 by nitrogen gas. Dried lipids were re-dissolved in a few drops of chloroform/methanol (1:2,
404 vol/vol) and loaded on a TLC plate. Lipids were separated by developing the TLC plate first in

405 acetone and then in a mixture of chloroform, methanol and 25% ammonia solution (50:25:6,
406 vol/vol/vol). Radiolabeled lipids were detected on a Storm 825 Phosphor-Imager (GE Healthcare).
407 **Generation of Lentivirus.**
408 Lentivirus production was performed as described previously[45]. Briefly, lentivirus was pro-
409 duced by co-transfection of HEK 293T cells with the pCDH-sgRNA/pCW-Cas9 and psPAX2 and
410 pMD2.G. Transfection was performed with Lipofectamine 3000 (Thermo Fisher) according to
411 manufacturer's instructions. Cells were cultured in DMEM supplemented with 10%FBS and the
412 growth medium was replaced after 6 hours. 48 hours after transfection, lentivirus-containing su-
413 pernatant was harvested, centrifuge for 5mins at 1250 rpm and filtered through a 0.45µm filter.
414
415 **Generation of CRISPR/Cas9-mediated Sptlc2-/- Raw264.7 cell line.**
416 Raw264.7 cells were infected with lentivirus (pCW-Cas9) encoding Cas9 cDNA, and were
417 cultured in media containing 7 µg/mL of puromycin (Sigma Aldrich). Potential target sequences
418 for CRISPR interference were found with the rules outlined in Mali et al. 2013[46]. The following
419 seed sequences (CRISPR target sequences) preceding the PAM motif that were found in the exon
420 of Sptlc2 gene were used: Sptlc2 #1 GAACGGCTGCGTCAAGAAC; Sptlc2 #2: AGCAGCAC-
421 CGCCACCGTCG Potential off-target effects of the seed sequence were evaluated using the NCBI
422 Mus musculus Nucleotide BLAST. Generation of CRISPR/Cas9-mediated Sptlc2-knockout
423 Raw264.7 cell line was performed as previously described[45]. Briefly, CRISPR gBlock was de-
424 signed to clone into the restriction enzymatic site NheI/BamHI of pCDH-CMV(-) (SBI; CD515B-
425 1) as follows:
426 cacagtcagacagtgactcaGTGTCACAgctagcTTTCCCATGATTCCTTCATATTTGCATA-
427 TACGATACAAGGCTGTTAGAGAGATAATTAGAATTAATTTGACTGTAAACACAAAG

428 ATATTAGTACAAAATACGTGACGTAGAAAGTAATAATTTCTTGGGTAGTTTGCAG-
429 TTTTAAAATTATGTTTTAAAATGGACTATCATATGCTTACCGTAACTTGAAAGTATTT
430 CGATTTCTTGGCTTTATATATCTTGTGGAAAGGACGAAACAC-
431 CGnnnnnnnnnnnnnnnnn-
432 nGTTTTAGAGCTAGAAATAGCAAGTTAAAATAAGGCTAGTCCGTTATCAACTTGAAA
433 AAGTGGCACCGAGTCGGTGCTTTTTTTggatccTGTGCACAgtcagtcacagtcagtctac (n:
434 CRISPR target sequences).

435 The gBlock was then digested using the restriction enzymes NheI and BamHI and ligated
436 into pCDH-CMV(-) vector that was linearized by digesting with the same restriction enzyme.

437 The Cas9-inducible cells were infected with lentivirus carrying pCDH-CMV(-)-sgRNA,
438 and were cultured in media containing 250 μg/mL of hygromycin B (Life Technology). To induce
439 expression of Cas9, cells were treated with 2 μg/mL of doxycycline (Clontech) for 3–5 days.
440 Clonal selection was performed by single cell dilution on 96-well plates. The individual colonies
441 were collected and the expression of Sptlc2 was examined by western-blotting using Sptlc2 anti-
442 body.

443 **U937 SGMS1 -/- cell lines**

444 U937 SGSM1 -/- cells were kindly provided by Sebastian Virreira Winter (Max Plack Insi-
445 tute) and the CRISPR/Cas9-mediated knock out cell lines were established as described in Winter
446 et al., 2016[39].

447 **Culturing of Mtb**

448 Culturing and infection of Mtb was conducted in a Biosafety-level 3 laboratory following
449 general safety guidelines. *M.tb* strain H37R, expressing constitutively mCherry, was cultured at
450 37°C in 7H9 Broth medium supplemented with 50μg/ml hygromycin B.

451 **Infection of macrophages with Mtb**

452 For infection of THP-1 and U937 cells, the cells were seeded into a SensoPlate™ 96-Well
453 Glass-Bottom Plates (Greiner Bio-One) at a density of $1.5x10^4$ cells per well in RPMI supple-
454 mented with 10% FBS, 1% Pen Strep and 50ng/ml PMA at 37°C. One day after differentiation
455 THP-1 cells were treated for 3 days with 5µM myriocin or 15µM fumonisin B1. Infection with
456 *M.tb* was performed after three days of differentiation of U937 cells and three days of drug treat-
457 ment of differentiated THP-1 cells. THP-1 and U937 cells were infected with a multiplicity of
458 infection (MOI) of 10 in RPMI supplemented with 10% FBS for 4 hours at 37°C.

459 For infection of Raw264.7 and DC2.4 cells, $2.0x10^4$ cells / well were seeded 24 hours prior
460 infection into a SensoPlate™ 96-Well Glass-Bottom Plates (Greiner Bio-One) and cultured in
461 RPMI 10%FBS, 1%Pen Strep at 37°C. Raw264.7 and DC2.4 cells were infected with a MOI of
462 10 in RPMI supplemented with 10% FBS for 4 hours at 37°C.

463 After 4 hours *M.tb* containing supernatant was aspirated, cells were washed one time with
464 PBS, and then fixed with 4% PFA over night at 4°C.

465 **Infection of macrophages with Herpes Simplex Virus-1**

466 Frozen, titered HSV-1-mCherry reporter virus was kindly provided to us by the lab of Dr.
467 David Johnson. Twenty-four hours prior to infection, $1x10^4$ wildtype and Sptlc2 knockout RAW
468 264.7 cells were seeded on glass coverslips in a 12-well plate. Cells were equally infected at an
469 MOI < 1, and incubated for 12 hours at 37°C and 5% CO_2. Coverslips were removed from plate
470 and fixed for 20 mins in 4% paraformaldehyde before staining with Alexa488-Phalloidin and
471 DAPI; slips were then imaged on a Keyence BZ-X700 and infection rates were calculated by au-
472 tomated cell counting, with Alexa488-phalloidin demarcating cell boundaries, DAPI staining for
473 nuclei counting, and mCherry expression for positive infection. Cells remaining in 12-well plate

474 following coverslip removal were lifted from the plate using 1x Trypsin (0.25%), washed with
475 PBS, and stained with 1:200 Zombie Aqua™ Dye for 30 mins on ice. Cells were then fixed for 20
476 mins in 4% paraformaldehyde, resuspended in FACS buffer (1x PBS, 3% FCS, 1mM EDTA), and
477 analyzed using an LSR-II flow cytometer, with uninfected, Live/Dead-stained and -unstained cells
478 as control.

479 **Microscopy**

480 Confocal microscopy was performed using an LSM880 microscope (Zeiss, Oberkochen,
481 Germany) using the PLAN APO for AiryScan 63x oil immersion objective, under the control of
482 the Zeiss Zen Blue software. Spinning disk confocal (SDC) imaging was performed on a Yoko-
483 gawa CSU-W1 SDC microscope (Nikon, Tokyo, Japan) using a 20x Plan Apo VC (NA 0.75) ob-
484 jective and a 60x Plan Apo VC (NA 1.4) oil immersion objective equipped with a Andor's Zyla
485 sCMOS camera under the control of the Nikon acquisition software and a stage motorized in
486 X,Y. Live cell imaging was performed at 37°C and 5% CO_2 using multi-position imaging with
487 automated focus at each time point. Representative images were analyzed and prepared using the
488 FIJI software.

489 Further quantitative imaging was performed on a Keyence BZ-X700 all in one fluorescence
490 microscope (Keyence Corporation, Osaka, Japan) using a SuperFluor 40.00xH oil immersion ob-
491 jective [PlanFluor and a 10x air-immersion objective], and controlled using the Keyence BZ-X
492 Viewer software. Image analysis and cell counting was performed using Keyence BZ-X Analyzer
493 software and FIJI.

494 **Phagocytosis assay**

495 Phagocytosis assay was performed as previously described[47]. Briefly, fixed cells were
496 washed twice with PBS and incubated in PBS for 15 min in Permeabilization Buffer (0.1% Triton

497 X-100 and 1%BSA). Cells were stained with Phalloidin-Alexa 488 (Thermo Fisher) at a final con-
498 centration of 33nM for 60 min and washed one time with PBS. After the Phalloidin-staining, cells
499 were stained with 1xDAPI for 10 mins and washed 3 times with PBS. THP-1 cells were then
500 imaged using the SDC microscope (Nikon) with a 20x objective and the U937, Raw264.7 and
501 DC2.4 cells were imaged with the Keyence BZ-X700 with a PlanFluor 20x objective. The param-
502 eters for imaging were kept the same for each sample. For image analysis either the Nikon or
503 Keyence BZ-X Analyzer software was used. In brief: The outline of the cells was determined via
504 the A488 signal (Phalloidin staining) and the number and area of mCherry (Mtb) signal in the
505 A488 signal was detected by the program. In a second round the number of cells was determined
506 by counting the nuclei via the DAPI staining. Number of bacteria (by mCherry-signal) inside the
507 cell was divided by the number of cells analyzed to identify the phagocytosis efficiency.

508 **Live imaging of phagocytosis**

509 For transient transfection, Raw264.7 cells were seeded into a SensoPlate™ 96-Well Glass-
510 Bottom Plates at a cell number of $1.0x10^4$ cells/well 24 hours prior transfection. Transfection was
511 conducted with Lipofectamine 3000 (Thermo Fisher) according to manufacturer's instructions.
512 Briefly, 100ng of plasmid DNA and 0.2µl of P3000 reagent were mixed in 5µl Opti-MEM and
513 0.33µl Lipofectamine 3000 was mixed in 5µl Opti-MEM. Both reagent dilutions were mixed to-
514 gether and allowed to sit for 15 min. The mix was then added directly to the appropriate well and
515 mixed by swirling the plate gently.

516 For imaging, the growth medium was aspirated and replaced with RPMI without phenol
517 red containing Zymosan A Bioparticles Alexa595 (Thermo Fisher) at an MOI of 20. The 96-well

518 plate were centrifuged at 1000rpm for one minute. The cells were imaged with the SDC micro-
519 scope (Nikon) and 3-4 different spots per well were imaged at the same time for 60 min with
520 capture intervals of 15 sec. The parameters for imaging were kept the same for each sample.

521 **Live imaging analysis**

522 Of live cell images, individual images were selected for further analysis if they captured a
523 cell bound to a zymosan particle while maintaining a healthy morphology throughout the imaging
524 time-course. Imaging analysis was performed using FIJI software[48]. The parameters for image
525 processing were kept constant when comparing different data sets. The area of the phagosome was
526 selected, cropped and opened in a new window. For the original image, the threshold was set au-
527 tomatically on the GFP-channel and for the threshold of the GFP-phagosome area, the threshold
528 of the whole cell was multiplied by 1.5 to ensure that only an increase in signal is counted (GFP-
529 threshold cell x 1.5 = GFP-threshold phagosome area). The threshold area at different time points
530 was measured by the analyze-measure function of FIJI and the results were exported into Excel
531 (Microsoft). The values for the GFP-threshold of the phagosome area were divided by the values
532 for the GFP-threshold of the whole cell at the corresponding time points.

533 **Dectin-1 transfection and co-localization**

534 Raw264.7 WT and *Sptlc2*$^{-/-}$ cells were seeded on glass coverslips in 12-well plates and
535 grown to 70-90% confluency overnight. The next day, cells were transfected with pMXsIP Dec-
536 tin-1-GFP using Lipofectamine 3000 (Invitrogen) according to the manufacturer's instructions.
537 After 24 hrs, cells were washed three times with ice-cold PBS, kept on ice for 5 min, and inocu-
538 lated with Alexa Fluor 594-conjugated zymosan in chilled serum-free DMEM at a ratio of 10
539 beads per cell. After centrifugation for 5 min at 250 x g and 4°C, cells were incubated for 5 min

540 at 37°C, washed three times with ice-cold PBS to remove unbound zymosan, then fixed for 15
541 min with 4% paraformaldehyde.

542 **Surface staining and flow cytometry**

543 RAW 264.7 wildtype and Sptlc2-/- cells were seeded on a T-75 culturing flask and grown in
544 parallel for three days. Cells were rinsed with PBS and lifted from the flask using treatment with
545 1x TryplE (ThermoFisher Scientific) for 10 mins. In a 96-well plate, on ice for 30 mins, Fc re-
546 ceptor was blocked with CD16/32 antibody (1:100) and cells were stained with ZombieAqua
547 Live/Dead (1:200). Cells were then stained with either CD45-APC (1:200), or Dectin-1-FITC
548 (1:50) for 30 mins. Finally, cells were fixed for 20 mins in 4% paraformaldehyde and analyzed
549 using an LSR-II flow cytometer. Cells independently stained with ZombieAqua, CD45-APC, and
550 Dectin-1-FITC were used for compensation. Analysis was performed using FlowJo software.

551

552

553 **References**

554

555 1. Daniel, T. M. The history of tuberculosis. *Respir. Med.* **100,** 1862–1870 (2006).

556 2. *Global tuberculosis report 2018.* (2018).

557 3. Korb, V., Chuturgoon, A. & Moodley, D. Mycobacterium tuberculosis: Manipulator of

558 Protective Immunity. *Int. J. Mol. Sci.* **17,** 131 (2016).

559 4. Ouimet, M. *et al.* Mycobacterium tuberculosis induces the miR-33 locus to reprogram

560 autophagy and host lipid metabolism. *Nat. Immunol.* **17,** 677–686 (2016).

561 5. Fine-Coulson, K., Reaves, B. J., Karls, R. K. & Quinn, F. D. The Role of Lipid Raft

562 Aggregation in the Infection of Type II Pneumocytes by Mycobacterium tuberculosis.

563 *PLoS One* **7,** (2012).

564 6. Thompson, C. R. *et al.* Sphingosine Kinase 1 (SK1) Is Recruited to Nascent Phagosomes

565 in Human Macrophages: Inhibition of SK1 Translocation by Mycobacterium tuberculosis.

566 *J. Immunol.* **174,** 3551–3561 (2005).

567 7. Levin, R., Grinstein, S. & Schlam, D. Phosphoinositides in phagocytosis and

568 macropinocytosis. *Biochim. Biophys. Acta - Mol. Cell Biol. Lipids* **1851,** 805–823 (2015).

569 8. Tafesse, F. G. *et al.* Disruption of Sphingolipid Biosynthesis Blocks Phagocytosis of

570 Candida albicans. *PLoS Pathog.* **11,** 1–27 (2015).

571 9. Malik, Z. A. *et al.* Cutting Edge: Mycobacterium tuberculosis Blocks Ca2+ Signaling and

572 Phagosome Maturation in Human Macrophages Via Specific Inhibition of Sphingosine

573 Kinase. *J. Immunol.* **170,** 2811–2815 (2003).

574 10. Kinoshita, M., Suzuki, K. G. N., Murata, M. & Matsumori, N. Evidence of lipid rafts

575 based on the partition and dynamic behavior of sphingomyelins. *Chem. Phys. Lipids* **215,**

576 84–95 (2018).
577 11. García-Arribas, A. B., Alonso, A. & Goñi, F. M. Cholesterol interactions with ceramide
578 and sphingomyelin. *Chem. Phys. Lipids* **199,** 26–34 (2016).
579 12. El Alwani, M., Wu, B. X., Obeid, L. M. & Hannun, Y. A. Bioactive sphingolipids in the
580 modulation of the inflammatory response. *Pharmacol. Ther.* **112,** 171–183 (2006).
581 13. Hla, T. & Dannenberg, A. J. Sphingolipid Signaling in Metabolic Disorders. *Cell Metab.*
582 **16,** 420–434 (2012).
583 14. Taha, T. A., Mullen, T. D. & Obeid, L. M. A house divided: Ceramide, sphingosine, and
584 sphingosine-1-phosphate in programmed cell death. *Biochim. Biophys. Acta - Biomembr.*
585 **1758,** 2027–2036 (2006).
586 15. Hakomori, S. I. & Igarashi, Y. Functional role of glycosphingolipids in cell recognition
587 and signaling. *J. Biochem.* **118,** 1091–1103 (1995).
588 16. Hannun, Y. A. & Obeid, L. M. The ceramide-centric universe of lipid-mediated cell
589 regulation: Stress encounters of the lipid kind. *J. Biol. Chem.* **277,** 25847–25850 (2002).
590 17. Snider, A. J., Alexa Orr Gandy, K. & Obeid, L. M. Sphingosine kinase: Role in regulation
591 of bioactive sphingolipid mediators in inflammation. *Biochimie* **92,** 707–715 (2010).
592 18. Capasso, S. *et al.* Sphingolipid metabolic flow controls phosphoinositide turnover at the
593 trans -Golgi network. *EMBO J.* **36,** 1736–1754 (2017).
594 19. Hinkovska-Galcheva, V., Boxer, L., Mansfield, P. J., Schreiber, A. D. & Shayman, J. A.
595 Enhanced phagocytosis through inhibition of de novo ceramide synthesis. *J. Biol. Chem.*
596 **278,** 974–982 (2003).
597 20. Hinkovska-Galcheva, V., Boxer, L., Mansfield, P. J., Schreiber, A. D. & Shayman, J. A.
598 Enhanced Phagocytosis through Inhibition of de Novo Ceramide Synthesis. *J. Biol. Chem.*

599 **278,** 974–982 (2003).

600 21. Gatfield, J. & Pieters, J. Essential role for cholesterol in entry of mycobacteria into
601 macrophages. *Science* **288,** 1647–50 (2000).

602 22. Hanada, K. Serine palmitoyltransferase, a key enzyme of sphingolipid metabolism.
603 *Biochim. Biophys. Acta* **1632,** 16–30 (2003).

604 23. Gault, C., Obeid, L. & Hannun, Y. An overview of sphingolipid metabolism: from
605 synthesis to breakdown Introduction to Sphingolipid Metabolism. *Adv Exp Med Biol* **688,**
606 1–23 (2010).

607 24. Leier, H. C., Messer, W. B. & Tafesse, F. G. Lipids and pathogenic flaviviruses : An
608 intimate union. 1–7 (2018). doi:https://doi.org/10.1371/journal.ppat.1006952

609 25. Meivar-Levy, I., Sabanay, H., Bershadsky, A. D. & Futerman, A. H. The Role of
610 Sphingolipids in the Maintenance of Fibroblast Morphology. *J. Biol. Chem.* **272,** 1558–
611 1564 (2002).

612 26. Wisner, T. W., Sugimoto, K., Howard, P. W., Kawaguchi, Y. & Johnson, D. C.
613 Anterograde Transport of Herpes Simplex Virus Capsids in Neurons by both Separate and
614 Married Mechanisms. *J. Virol.* **85,** 5919–5928 (2011).

615 27. Tiwari, V. & Shukla, D. Nonprofessional Phagocytosis Can Facilitate Herpesvirus Entry
616 into Ocular Cells. *Clin. Dev. Immunol.* **2012,** 1–8 (2012).

617 28. Clement, C. *et al.* A novel role for phagocytosis-like uptake in herpes simplex virus entry.
618 *J. Cell Biol.* **174,** 1009–1021 (2006).

619 29. Gianni, T., Gatta, V. & Campadelli-Fiume, G. V 3-integrin routes herpes simplex virus to
620 an entry pathway dependent on cholesterol-rich lipid rafts and dynamin2. *Proc. Natl.*
621 *Acad. Sci.* **107,** 22260–22265 (2010).

622 30. Mao, Y. & Finnemann, S. C. Regulation of phagocytosis by Rho GTPases. *Small*
623 *GTPases* **6,** 89–99 (2015).
624 31. Schlam, D. *et al.* Phosphoinositide 3-kinase enables phagocytosis of large particles by
625 terminating actin assembly through Rac/Cdc42 GTPase-activating proteins. *Nat. Commun.*
626 **6,** 8623 (2015).
627 32. Hoppe, A. D. & Swanson, J. A. Cdc42, Rac1, and Rac2 Display Distinct Patterns of
628 Activation during Phagocytosis. *Mol. Biol. Cell* **15,** 3509–3519 (2004).
629 33. Underhill, D. M. Macrophage recognition of zymosan particles. *J. Endotoxin Res.* **9,** 176–
630 180 (2003).
631 34. Rothfuchs, A. G. *et al.* Dectin-1 Interaction with Mycobacterium tuberculosis Leads to
632 Enhanced IL-12p40 Production by Splenic Dendritic Cells. *J. Immunol.* **179,** 3463–3471
633 (2007).
634 35. Queval, C. J., Brosch, R. & Simeone, R. The Macrophage: A Disputed Fortress in the
635 Battle against Mycobacterium tuberculosis. *Front. Microbiol.* **8,** (2017).
636 36. Hanada, K. *et al.* Molecular machinery for non-vesicular trafficking of ceramide. *Nature*
637 **426,** 803–809 (2003).
638 37. Marshall, J. G. *et al.* Restricted accumulation of phosphatidylinositol 3-kinase products in
639 a plasmalemmal subdomain during Fcγ receptor-mediated phagocytosis. *J. Cell Biol.* **153,**
640 1369–1380 (2001).
641 38. Subbaiah, P. V. & Sargis, R. M. Sphingomyelin: A natural modulator of membrane
642 homeostasis and inflammation. *Med. Hypotheses* **57,** 135–138 (2001).
643 39. Virreira Winter, S., Zychlinsky, A. & Bardoel, B. W. Genome-wide CRISPR screen
644 reveals novel host factors required for Staphylococcus aureus α-hemolysin-mediated

645 toxicity. *Sci. Rep.* **6,** 24242 (2016).

646 40. Goodridge, H. S. *et al.* Activation of the innate immune receptor Dectin-1 upon formation
647 of a 'phagocytic synapse'. *Nature* **472,** 471–475 (2011).

648 41. Grassmé, H. *et al.* Host defense against Pseudomonas aeruginosa requires ceramide-rich
649 membrane rafts. *Nat. Med.* **9,** 322 (2003).

650 42. Hauck, C. R. *et al.* Acid sphingomyelinase is involved in CEACAM receptor-mediated
651 phagocytosis of Neisseria gonorrhoeae. *FEBS Lett.* **478,** 260–266 (2000).

652 43. Feng, S. *et al.* A Rapidly Reversible Chemical Dimerizer System to Study Lipid Signaling
653 in Living Cells. *Angew. Chemie Int. Ed.* **53,** 6720–6723 (2014).

654 44. BLIGH, E. G. & DYER, W. J. A rapid method of total lipid extraction and purification.
655 *Can. J. Biochem. Physiol.* **37,** 911–7 (1959).

656 45. Tafesse, F. G. *et al.* GPR107, a G-protein-coupled Receptor Essential for Intoxication by
657 Pseudomonas aeruginosa Exotoxin A, Localizes to the Golgi and Is Cleaved by Furin. *J.*
658 *Biol. Chem.* **289,** 24005–24018 (2014).

659 46. Mali, P. *et al.* RNA-guided human genome engineering via Cas9. *Science* **339,** 823–6
660 (2013).

661 47. Rashidfarrokhi, A., Richina, V. & Tafesse, F. G. Visualizing the Early Stages of
662 Phagocytosis. *J. Vis. Exp.* (2017). doi:10.3791/54646

663 48. Schindelin, J. *et al.* Fiji: an open-source platform for biological-image analysis. *Nat.*
664 *Methods* **9,** 676–682 (2012).

665

666

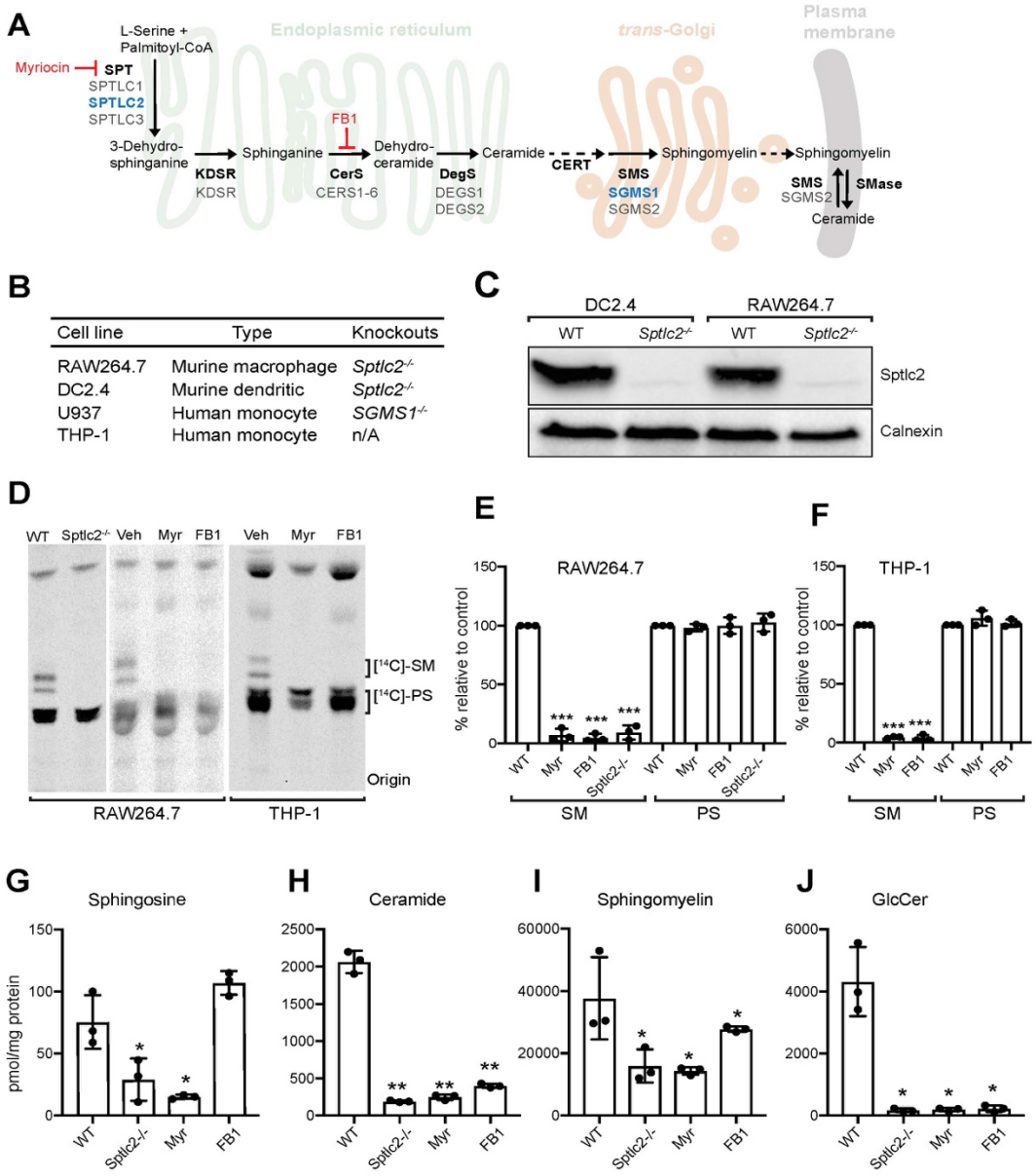

Figure 1: Manipulation of cellular sphingolipid levels using genetics and chemical tools. (A) Simplified overview of sphingolipid biosynthetic pathway. Genes that are deleted using CRISPR/Cas9 system are indicated in blue and the inhibitors that are used in this study are shown in red. (B) Model phagocyte cell lines used in this study, respective species background, and genetic knockouts available. (C) Western blot probed using anti-Sptlc2 antibody in wildtype and CRISPR/Cas-9 knockout DC 2.4 and RAW 264.7 cells (upper), and probed against calnexin as loading control (lower). (D) Control, mutant and inhibitor-treated cells were labeled with the sphingolipid precursor 3-L-[^{14}C]-serine, and total lipids were extracted and analyzed by thin layer chromatography (TLC) and autoradiography. (E, F) Quantification of the [^{14}C]-SM and [^{14}C]-PS signals from [^{14}C]-serine labeling of RAW264.7 and THP-1 cells shown in *D*. (G-J) Total lipids were extracted from control, Sptlc2-/- and inhibitor-treated cells and lipid profiling was performed using LC/MS. Levels of sphingosine (G), ceramide (H), sphingomyelin (I) and glucosylceramide (GlucCer) are shown. All graphs display SD of three independent experiments, and an unpaired t-test was used to analyze the significance of the data. *$p<0.05$, **$p<0.01$, *** $p < 0.001$.

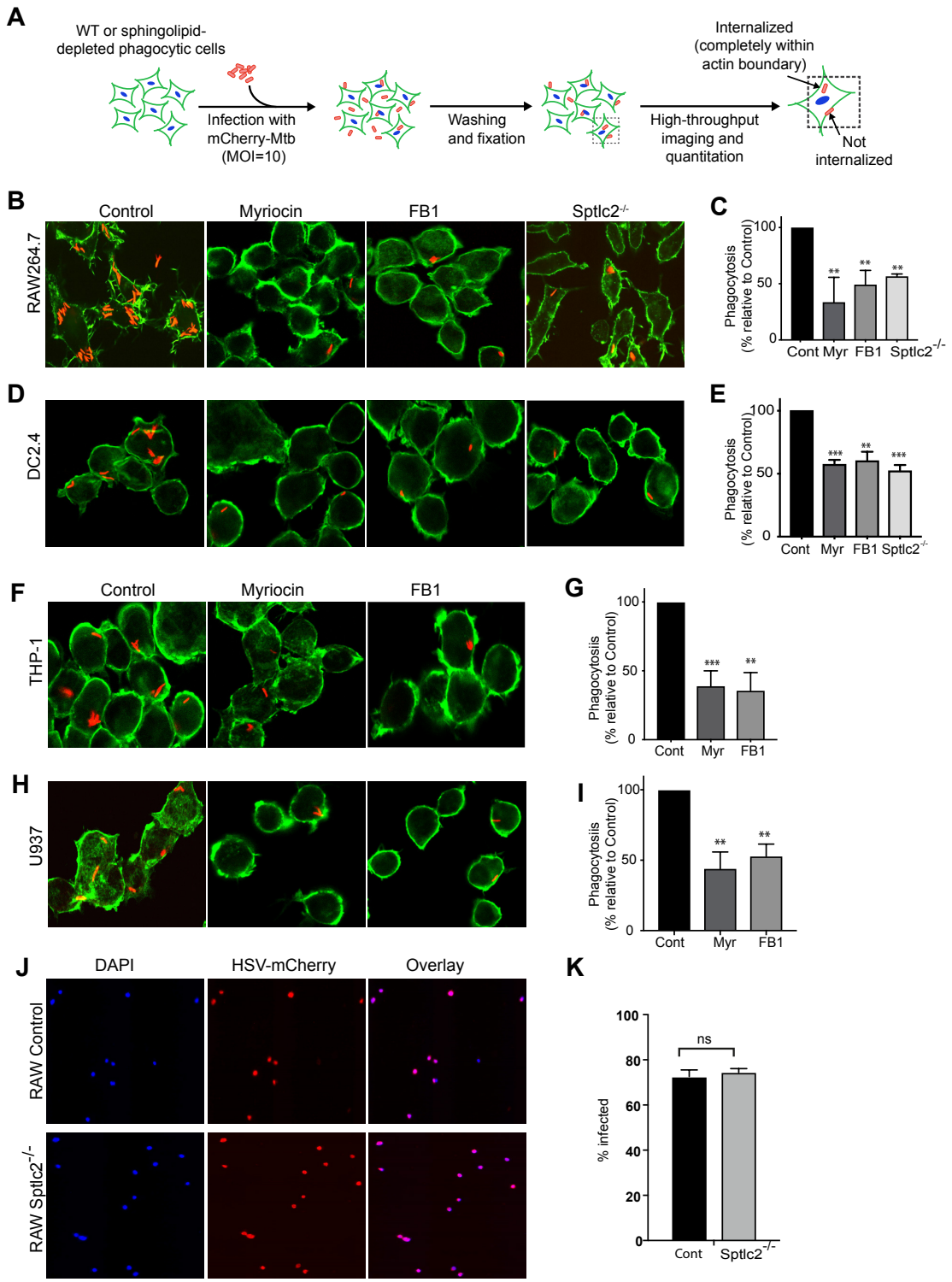

681

682 **Figure 2: Sphingolipid biosynthesis is required for efficient phagocytosis of Mtb.**
683 A) Overview of the phagocytosis experiment. (B, D) Representative images of Mtb-infected
684 RAW 264.7 (B) and DC 2.4 (D) cells. (C, E) Quantification of Mtb uptake in RAW 264.7 (C)

685 and DC2.4 (E) cells over three independent biological replicates, with at least 1,000 cells quanti-
686 fied per replicate. Mtb uptake was defined using total number of bacteria (mCherry signal)
687 within cellular periphery (Phalloidin-Alexa488 signal) and cellular counts were defined by nu-
688 clear stain. (E, H) Representative images of infected THP-1 (F) and U937 (H) monocyte-derived
689 macrophages. $2x10^4$ THP-1 and U937 cells were plated in 96-well plate and were differentiated
690 using 80ng/ml PMA for one day, and then treated for three days with 5µM myriocin or 15µM
691 fumonisin B1. (G, I) Quantification of Mtb uptake in THP-1 (G) and U937 (I) cells. (J) Micros-
692 copy images of cells that were infected with HSV-RFP (MOI of 10). At 12 h post infection, cells
693 were fixed, stained with DAPI and analyzed by microscopy. (K) Quantification of experiments
694 performed as described in C. n = 3 independent experiments. Data are mean ± SD. *p<0.05,
695 **p<0.01, ***p<0.001, two-tailed unpaired t-test.
696
697
698
699

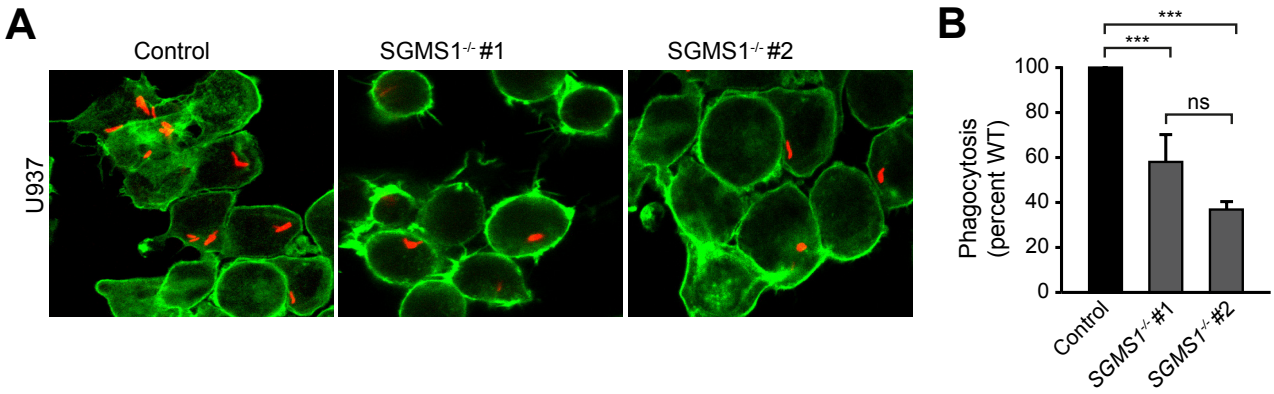

700

701 **Figure 3: Sphingomyelin is essential for phagocytosis of Mtb, but not for HSV entry**
702 (A) Representative images of Mtb-infected wildtype and two clonal isolates of SGMS1
703 CRISPR/Cas9 knockout U937 cells generated using two independent sgRNAs. Cells were acti-
704 vated with 80nM PMA for 48 h before Mtb infection. (B) Quantification of Mtb uptake over
705 three independent biological replicates, with at least 1,000 cells quantified per replicate. Data are
706 mean ± SD. ns = not significant, ***p<0.001, two-tailed unpaired t-test.
707

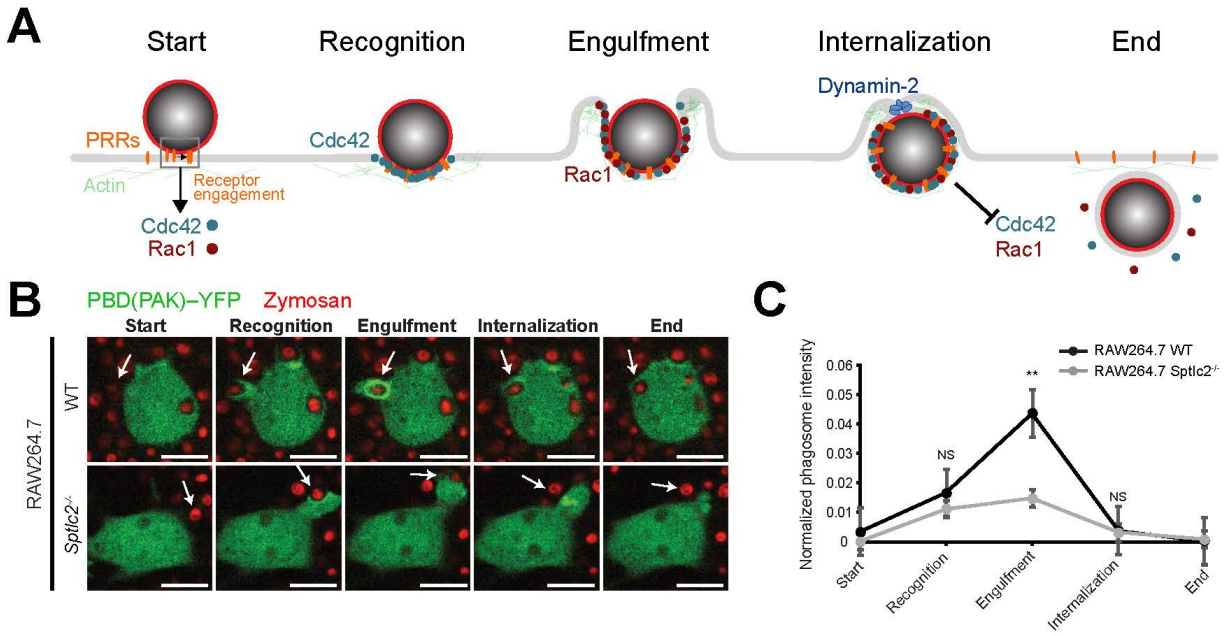

Figure 4. Sphingolipids are essential for efficient recruitment of Cdc42/Rac1 to the phagocytic cup. (A) Schematic representation of the small GTPase Cdc42 and Rac1 role during phagocytosis. (B) Confocal images of wild type and Sptlc2-/- RAW264.7 macrophages transfected with PAK(PBD)–GFP, a biosensor for active Rac/Cdc42, during phagocytosis. Cells were incubated with Alexa Fluor 594-conjugated zymosan A particles, and live imaging was performed. Images captured at 30-second intervals are shown. (C) A graph showing quantitation of the PAK(PBD) fluorescence intensity in the course of formation of a phagocytic cup (shown in arrow) as performed in B. All graphs display SD of three independent experiments, and an unpaired t-test was used to analyze the significance of the observed differences. ** $p < 0.01$.

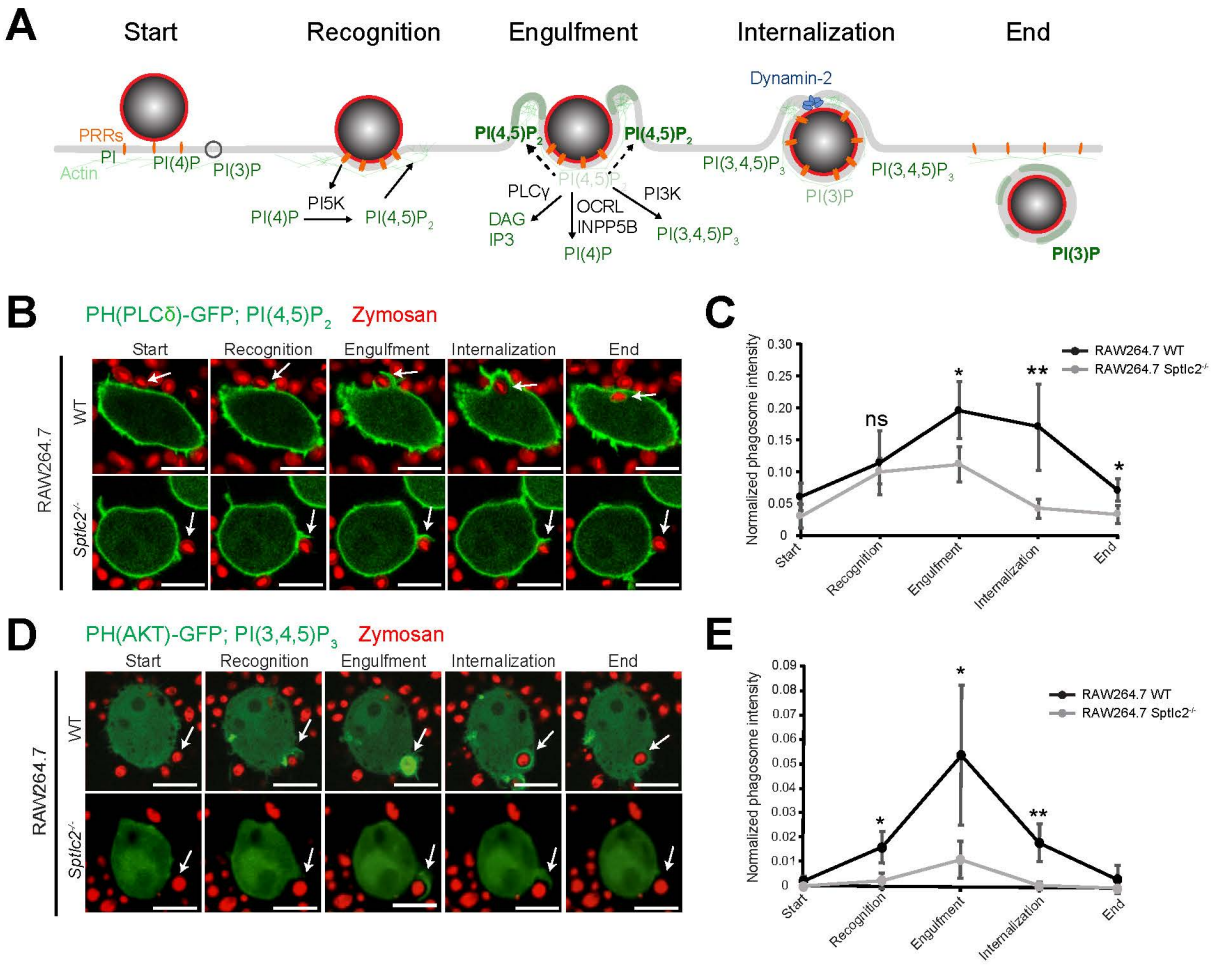

Figure 5: Phosphoinositide turnover dynamics are disrupted in sphingolipid-deficient phagocytes. (A) Schematic depiction of phosphoinositide dynamics during phagocytosis. (B, D) Time-lapse confocal microscopy images of wildtype and Sptlc2$^{-/-}$ RAW 264.7 cells expressing PH(PLCδ)-GFP, the PI(4,5)P_2 biosensor (B) or PH(AKT)-GFP, the (PI3,4,5)P_3 biosensor (D) after infection with Alexa Flour 594 conjugated zymosan A particles at MOI of 10. Representative images that are captured at 30-second intervals are shown. (C, E) Accumulation of GFP signal to site of particle binding was quantified by the ratio of GPF signal intensity at phagosome versus GFP signal across entire cell at the indicted time points for experiments performed as *B* and *D*. n= 3 independent experiments and the mean GFP intensity profiles of 10 - 20 cells are represented. Data are mean ± SD. *p<0.05, **p<0.01, ***p<0.001, two-tailed unpaired t-test, ns = not significant

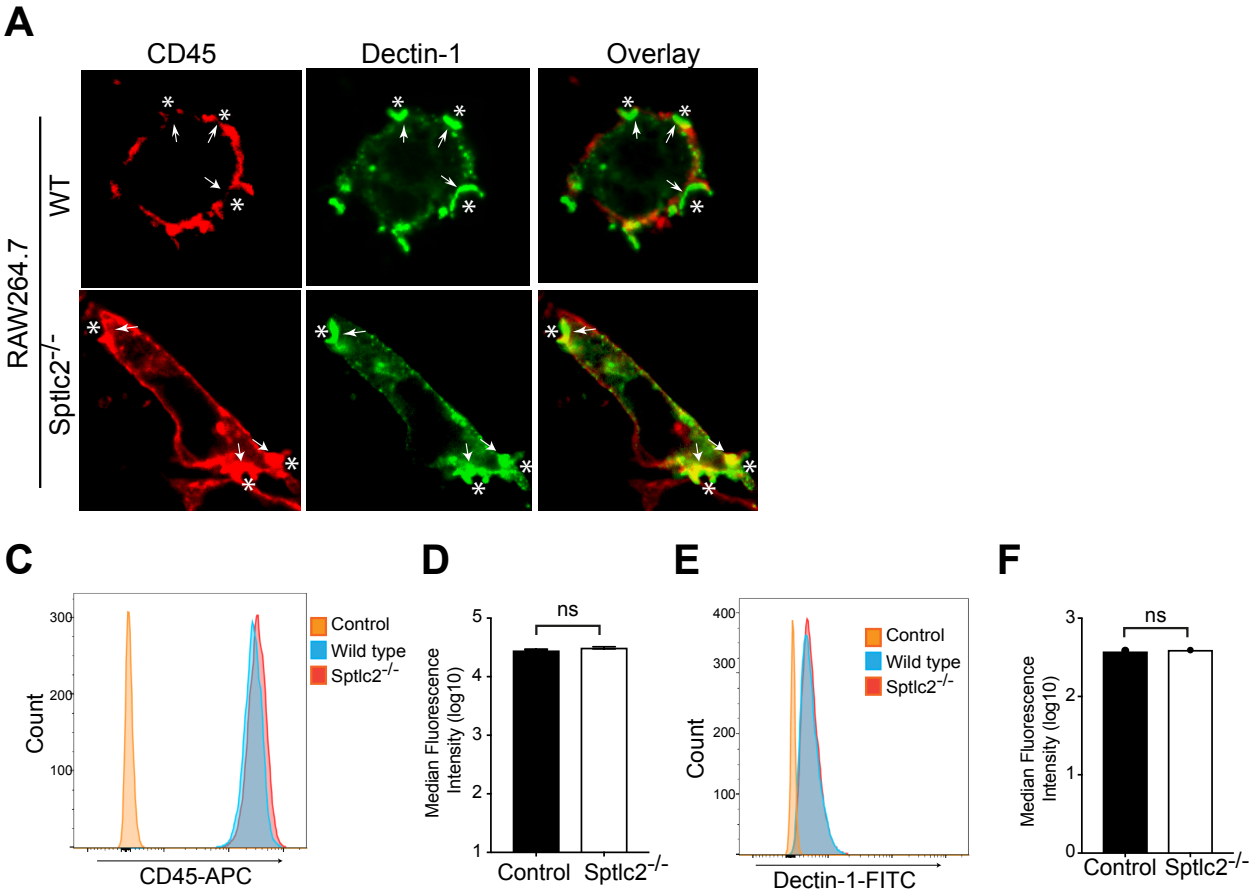

732

733 **Figure 6: Exclusion of CD45 by Dectin-1 from cup formation site is impaired in Sptlc2$^{-/-}$**
734 **cells.** (A) Confocal microscopy of GFP-tagged Dectin-1-expressing RAW264.7 macrophages
735 stimulated with zymosan for 2 min and stained for CD45 (red). Zymosan particles are shown in
736 star (*) at the phagocytic cup. (B) Quantitation of the level of CD45 and Dectin-1 at the site of
737 contact. (C, E) Flow cytometry of CD45 and Dectin-1at the cell surface of Sptlc2-/- and control
738 RAW264.7 macrophages. (D, F) Graphs showing quantification of cell surface expression of the
739 receptors described in C and E, respectively. All data are representative of 3 independent experi-
740 ments. Data are mean ± SD. ns = not significant, two-tailed unpaired t-test.
741

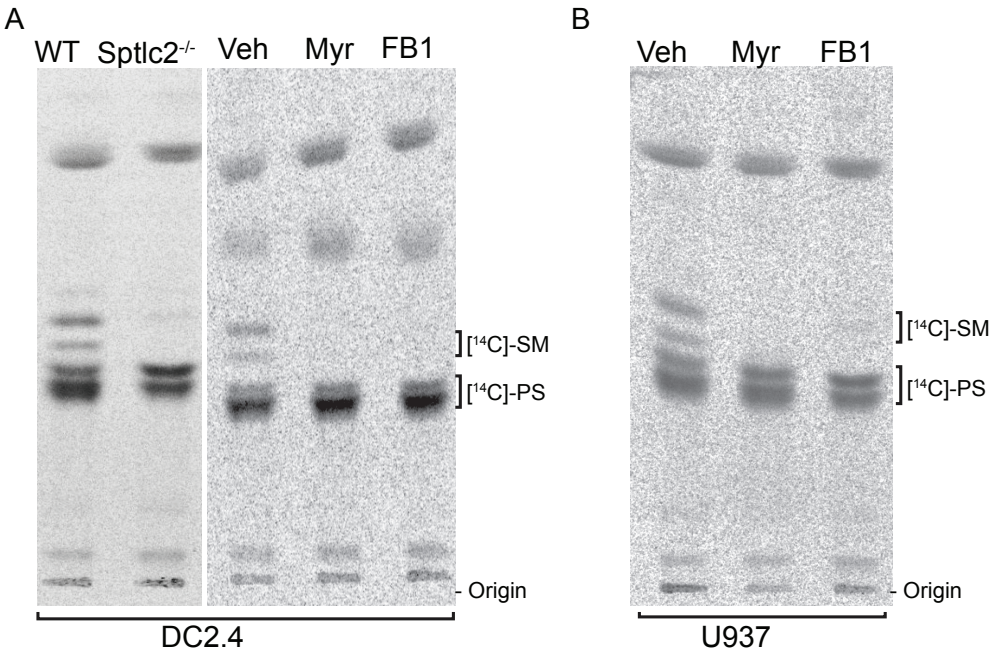

742

743 **Supplemental Figure 1: Genetic and small molecule inhibitors mediated depletion of sphin-**
744 **golipid in phagocytes**
745 (A, B) Control, mutant and inhibitor-treated cells were labeled with the sphingolipid pre-
746 cursor 3-L-[^{14}C]-serine, and total lipids were extracted and analyzed by thin layer chromatog-
747 raphy and autoradiography. All data are representative of 3 independent experiments.
748

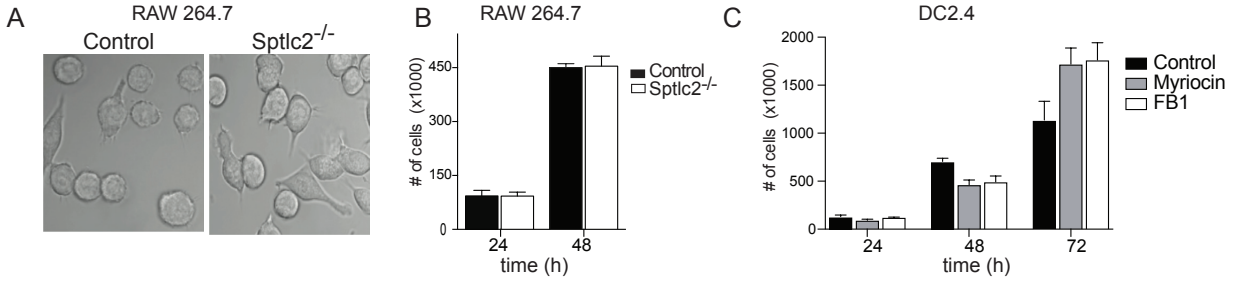

Supplemental Figure 2: Depletion of sphingolipids has no effect on cell morphology, growth rate or cell division. (A) Microscopy images of control and Sptlc2-/- RAW 264.7 macrophages, showing no morphological difference between the mutant and control cells. (B, C) The cell division of the control and Sptlc2-/- RAW 264.7 macrophages (B), and inhibitor treated DC2.4 cells (C) at different time points was measured and presented.